Catalysis Today 149 (2010) 295–303

Contents lists available at ScienceDirect

Catalysis Today

journal homepage: www.elsevier.com/locate/cattod

CO and NO adsorption for the IR characterization of Fe^{2+} cations in ferrierite: An efficient catalyst for NOx SCR with NH_3 as studied by *operando* IR spectroscopy

I. Malpartida [a], E. Ivanova [b], M. Mihaylov [b], K. Hadjiivanov [b], V. Blasin-Aubé [a], O. Marie [a,*], M. Daturi [a]

[a] Laboratoire Catalyse et Spectrochimie, ENSICAEN, Université de Caen, CNRS, 6 bd. Maréchal Juin, 14050 Caen Cedex, France
[b] Institute of General and Inorganic Chemistry, Bulgarian Academy of Sciences, Sofia 1113, Bulgaria

ARTICLE INFO

Article history:
Available online 30 October 2009

Keywords:
Ferrierite
SCR-NH_3
CO and NO adsorption
In situ IR
Operando IR

ABSTRACT

Iron was introduced by ionic exchange inside the FER structure in order to yield a Fe-FER series with increasing metal loading. Characterization of the Fe^{2+} cations by adsorption of CO at liquid nitrogen temperature followed by infrared spectroscopy allowed to identify three distinct sites for iron. The most abundant iron species are located on easily accessible sites of the FER structure, whereas high metal loading is required to observe more confined Fe^{2+} species. According to the CO adsorption results, the main iron species appears to be coordinatively unsaturated whereas isotopic labelling upon NO adsorption indicates that two distinct iron sites almost give rise to the same mononitrosyl infrared signature. Studying the catalyst upon interaction with NO and O_2 in *operando* conditions leads to the observation of these mononitrosyl species who behave as reaction intermediates for the NO oxidation into NO_2. All our Fe-FER samples presenting these mononitrosyl complexes are active not only in NO-to-NO_2 reaction but also in the NOx selective catalytic reduction with ammonia. The effects of both NH_3 and SO_2 as adsorption competitor during the low temperature NH_3-SCR are also discussed.

1. Introduction

The growing environmental regulations have forced the development of lean-burn engines that offer a reduction in fuel consumption and in CO_2 emissions. In these conditions of oxygen excess, selective catalytic reduction (SCR) using hydrocarbons or ammonia as reducing agent permits the NOx abatement [1].

Zeolite-based catalysts can be particularly effective for the selective catalytic reduction of NO with methane or propene [2]. In particular, Fe-containing zeolites are reported to be effective catalysts in various reactions such as selective catalytic reduction of nitrogen oxides with hydrocarbons or ammonia. Taking into account that iron sites provide the red–ox centres, the properties of exchanged Fe cations for NO oxidation depend not only on the type of zeolite but also on their location in the structure.

In situ IR spectroscopy study of adsorbed probe molecules, especially of CO, is very useful for the characterization of solid surfaces and gives a unique possibility to characterize the coordination state and electrophilic properties of accessible cations in zeolites [3]. In addition, on the basis of the so-called "confinement" effect, cations located in big and small cavities could be discriminated [4]. Besides, it is interesting to investigate materials and processes under operating conditions as close as possible to real application conditions. The "Laboratoire de Catalyse et Spectrochimie of Caen" currently works in the domain of IR spectroscopy and during the last two decades it has developed an IR reactor cell that enables the analysis of the gas phase and the catalytic surface simultaneously under operating conditions. This system, so-called *operando*, consists in an online MS-spectrometer providing the outlet gases analysis, coupled with an IR instrument that allows to take spectra from surface and gas phase alternatively [5,6]. The catalytic properties of iron-containing ferrierite under reaction conditions were investigated in this contribution. More precisely, the aim of this work was first to characterize exchanged Fe^{2+} cations in ferrierite (Fe-FER) by means of in situ IR spectroscopy and then to study for selected samples both their NO-to-NO_2 oxidation ability (in the presence and absence of SO_2) and their NOx SCR efficiency via *operando* methodology.

2. Experimental

Fe-FER samples were prepared from a mother NH_4^+-FER sample with Si/Al ratio = 8.8 by consecutive ionic exchanges from ferrous sulphate solutions followed by several washings with distilled water in order to remove any sulphate traces. The global cation exchange capacity for this mother sample can be estimated from the Si/Al ratio around 1.7×10^{-3} mol g^{-1} when considering a monovalent cation. The three '*x* wt% Fe-FER' used for this work (where *x* stands for the iron weight loading) are part of a larger series of samples for which more details are given in Ref. [7]. In

* Corresponding author. Tel.: +33 2 31 45 28 25; fax: +33 2 31 45 28 22.
E-mail address: olivier.marie@ensicaen.fr (O. Marie).

0920-5861/$ – see front matter © 2009 Elsevier B.V. All rights reserved.
doi:10.1016/j.cattod.2009.09.015

order to facilitate the comparison with other works from literature, one can also express the iron loading from the Fe/Al molar ratio. In our case, this leads to the following:

0.96 wt% Fe-FER corresponds to Fe/Al = 0.10.
2.5 wt% Fe-FER corresponds to Fe/Al = 0.27.
3.7 wt% Fe-FER corresponds to Fe/Al = 0.41.

CO and NO were purchased from Air Liquide, France with respective nominal purity of 99.997% and 99.9% whereas labelled ^{15}NO was provided by ONIA and 98.5% enriched. All probe molecules were further purified by trapping at liquid nitrogen temperature.

2.1. In situ IR

Material surface properties have been studied by in situ FT-IR spectroscopy of adsorbed probe molecules. Self-supporting pellets of around 10 mg cm^{-2} were prepared and analyzed in a classical quartz cell connected to a vacuum-adsorption apparatus for in situ experiments. Spectra were either recorded at liquid nitrogen or room temperature with a Nicolet Magna 550 FT-IR spectrometer (resolution 4 cm^{-1}).

For both CO and NO adsorptions, the Fe-FER samples were pre-treated by thermal activation at 673 K under dynamic vacuum. Regarding the CO experiment, the sample was surrounded with a Dewar filled with liquid nitrogen so that its temperature was measured to be around 100 K and further put in contact with an equilibrium CO pressure (200 Pa) followed by dynamic evacuation. In the case of NO adsorption, pure ^{15}NO was first introduced at room temperature with a corresponding equilibrium pressure of 133 Pa and then ^{14}NO was added via a calibrated volume in order to obtain a resulting equimolar mixture of ^{15}NO and ^{14}NO in contact with the Fe-FER sample. Finally the catalyst was heated to 423 K in order to favour the isotopic exchange. All spectra have been processed by the Nicolet OMNIC software.

2.2. Reaction system

Our *operando* system is connected to a flow set-up. Gases are introduced into the lines (heated at 333 K) by mass flow controllers and using argon as a carrier gas. Reactants can also be pulsed using a 0.004–0.020 cm^3 injection loop purged by one-tenth of the carrier flow. Two gas mixtures can be simultaneously prepared in our system (activation and reaction flow), and then alternately sent to the reactor cell described below. Our system allows the analysis of both the reactants and/or the reaction products by Quadrupole Mass Spectrometry (Balzers TCP 121), FT-IR spectroscopy (via a gas microcell of 0.088 cm^3 volume) and gas chromatography (Varian micro GC CP-4900). IR spectra are collected with a Nicolet Magna 750 FT-IR spectrometer, equipped with MCT detectors. In order to ameliorate the signal/noise ratio, the number of scans accumulation can be set to 64 at a resolution of 4 cm^{-1}. Decreasing the scans accumulation allows a time resolution of 1 s which is always the case for the QMS analysis. Micro GC, on the contrary, allows only periodic sampling, because time resolution corresponds to about one injection every 30 s. The simultaneous use of MS and IR gas cell allows us to discriminate species giving the same signal in mass spectra, such as NO and NO_2 (m/e = 30) or N_2 and CO (m/e = 28).

2.3. The reactor cell

Our home-made IR reactor cell is shown in Fig. 1: it consists of a stainless steel cylinder carrying a torroidal sample holder in its centre, where the self-supported wafer of catalyst is placed (6 mg cm^{-2}). The heating system guarantees a maximum temperature of 723 K on the sample, while the air cooling system keeps the two ends of the cell below 573 K, in such a way that the tightness (up to 30 bar) can be obtained by Kalrez O-rings between the terminal CaF_2 windows and the extremities of the cell. The rest of the space is filled with KBr windows, which limit the dead volume (the residual space between each sample face and

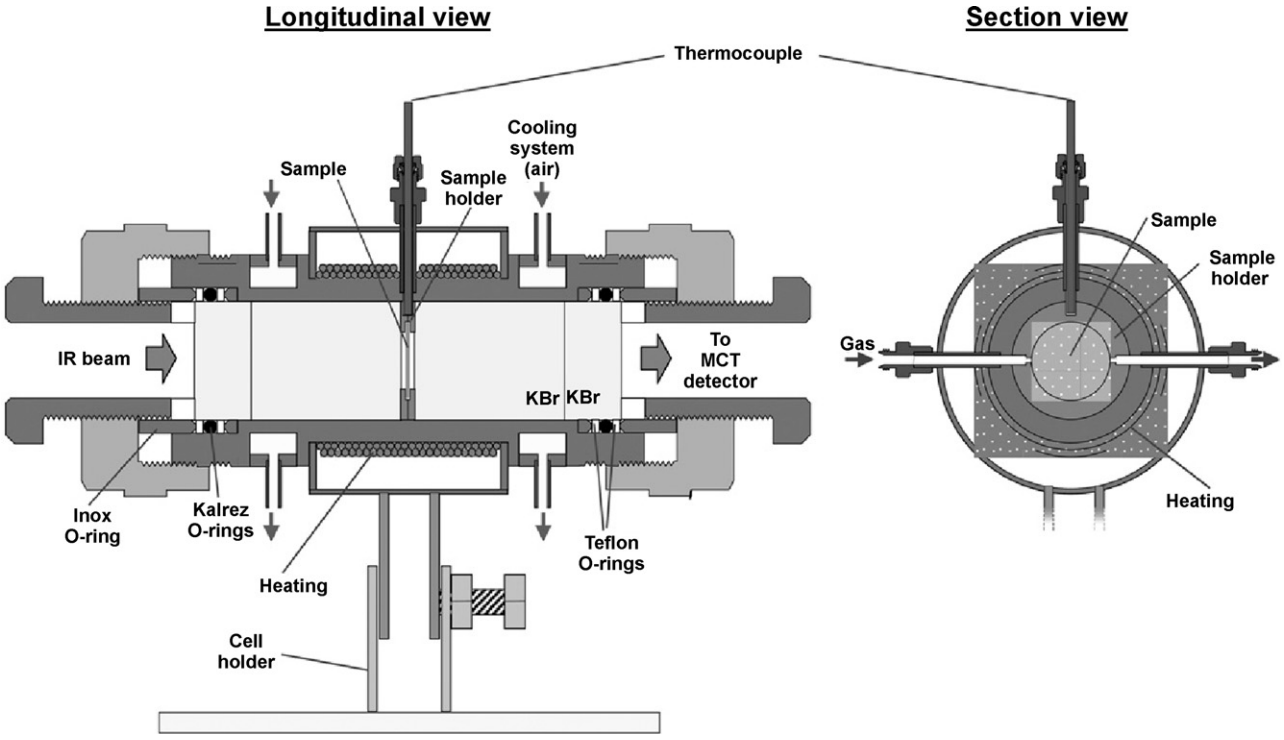

Fig. 1. Technical view of the *operando* IR reactor cell (figure reproduced by permission of the RCS from Ref. [5]).

windows) to 0.12 cm^3 and the optical path below 3 mm. This small dead volume and the fact that the gas leaches the wafer create flow conditions very similar to those in a monolith. The external windows can also be made of KBr or BaF_2 in order to widen the transparency range. The experiments are carried out at atmospheric pressure; gases are forced on the sample by 1/16 pipe and collected on the opposite side of the sample holder. In such a configuration the weight hourly space velocity (WHSV) can be adjusted in the range 40–400 h^{-1}.

2.4. Gas flow composition

The conditions for *operando* experiments are established at constant temperature T = 433 K with the following flow composition: 500 ppm of NO + 6% O_2 for the study of NO-to-NO_2 oxidation efficiency whereas the SCR study was performed either on the 'as-synthesized' NH_4^+ sample or by first reloading the sample with ammonia using 1000 ppm of NH_3 in argon before a mixture of 500 ppm of NO + 10% of O_2 in argon was sent to the catalyst. When desired, SO_2 (50 ppm) was added to the reacting gas mixture. Even if always present in any post-combustion exhaust gas, we decided not to add water in our reaction flow for the following reason: we aim at evidencing a potential competition adsorption effect between NO and NH_3 on iron sites during the SCR reaction. However, in zeolites the only vibration mode that is available to follow the presence of adsorbed ammonia onto Lewis sites (i.e. Fe cations in our case) is the $\delta(NH_3)$ bending, lying around 1600–1640 cm^{-1}, where adsorbed water is also detected with a much higher molar extinction coefficient.

3. Results and discussion

3.1. CO adsorption

Although carbon monoxide is one of the most used IR probe molecules, there are only few studies dealing with CO adsorption on iron-containing zeolites. Below we show that CO is a sensitive probe for the characterization of Fe^{2+} ions especially with the Fe-FER system. We present the spectra of CO adsorbed at 100 K in order to achieve a higher coverage and to detect all cationic sites able to form carbonyls. The feature of CO adsorption on two samples, having high and low iron concentration is described, the picture of the other samples being intermediate between these two border cases.

Adsorption of CO on the 3.7 wt% Fe-FER sample leads to the appearance in the IR spectrum of several carbonyl bands: at 2140 cm^{-1} (due to physically adsorbed CO), at 2173 cm^{-1} (assigned to CO adsorbed on zeolite bridging hydroxyls) and a rather broad band at 2188 cm^{-1} (Fig. 2, spectrum a). The latter band was not detected with the mother zeolite and is therefore assigned to carbonyls formed with participation of iron cations. Upon evacuation the band at 2188 cm^{-1} gradually transformed into a band at 2196 cm^{-1} (Fig. 2, spectra b–f). The latter easily vanished upon additional evacuation which evidences a weak, essentially electrostatic bond between the iron sites and CO. The result obtained can be explained by conversion of dicarbonyls (band at 2188 cm^{-1}) to monocarbonyls (band at 2196 cm^{-1}). Taking into account summarized literature data [3], we infer that the species observed are carbonyls of Fe^{2+} ions.

Note that, due to the similar stabilities of the mono- and dicarbonyls species, no clear isosbestic point is detected. The presence of one single band for the dicarbonyls is also expected: it is now well established that when the metal–CO interaction occurs by weak electrostatic bonding, the two CO molecules in the dicarbonylic species behave as independent oscillators and there is no split of the CO stretching modes [8–14]. Since there is no space

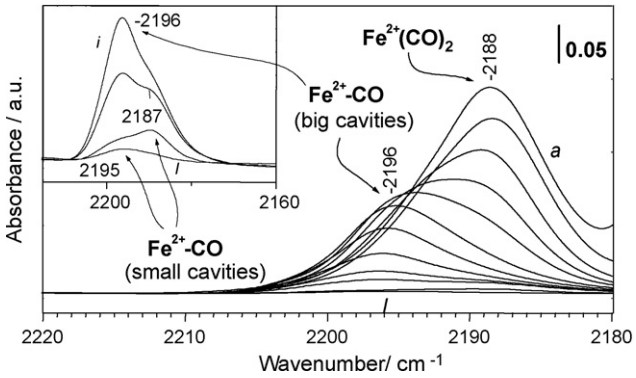

Fig. 2. IR spectra of CO at 100 K on a 3.7 wt% Fe-FER activated at 673 K. Equilibrium pressure of 200 Pa (a) and evolution of the spectra under dynamic vacuum ($b \rightarrow l$).

limitation to form geminal dicarbonyl species, we conclude that the corresponding iron sites are not located in a confined environment.

Upon dynamic evacuation two other bands with much lower intensities became visible at 2195 and 2187 cm^{-1} (see the inset in Fig. 2). Although the position of the band at 2195 cm^{-1} is close to the position of the intense band at 2196 cm^{-1}, the two bands characterize two types of carbonyls dramatically differing in stability. In principle, a higher stability of the carbonyls should correlate with a higher CO stretching frequency. This contradiction could find an easy explanation assuming that, with the 2195 and 2187 cm^{-1} species, CO undergoes interaction by both the C- and O-ends. It is well known, in fact, that bonding of CO through the oxygen atom leads to a decrease in the CO stretching frequency, thus compensating the blue shift due to the interaction via the C-end. Therefore, we suggest that the at 2195 and 2187 cm^{-1} carbonyls are formed with the participation of Fe^{2+} cations in smaller cavities or more locally confined sites, where CO from the Fe–CO species can interact through its O-end with other cations, e.g. Fe^{2+} or H^+, because of the close proximity between interacting entities. Such confinement effect would thus increase the carbonyl species stability without leading to a high CO stretching frequency, since CO interaction via both ends induces compensating effects. According to this interpretation, the 2195 cm^{-1} band would thus characterize the most confined carbonyl species.

For the 0.96 wt% Fe-FER the main iron carbonyl band was again at 2196 cm^{-1} (which converted to a dicarbonyl band at 2188 cm^{-1} at low temperature and CO equilibrium pressure). The 2187 cm^{-1} component had a lower intensity and the third 2195 cm^{-1} component was not detected.

We also like to note that quantitative measurements showed that the amount of iron sites detected by CO is lower that the total iron amount in the sample. This is in agreement with the presence of Fe^{3+}, as detected by Mössbauer spectroscopy [7], that are not able to form carbonyl complexes.

In conclusion, the results obtained show the existence of three types of Fe^{2+} sites in the FER structure which are gradually occupied upon consecutive ion exchange.

3.2. NO adsorption

Dealing now with the NO adsorption, we recently reported [7] that for the low loaded 0.96 wt% Fe-FER sample the interaction with NO leads to the appearance of a unique highly symmetric band at 1876 cm^{-1}, which is typical of Fe^{2+}–NO mononitrosyl species. However, we were not able using NO adsorption to identify two distinct signals as was observed above with this sample upon CO adsorption. Moreover, for NO adsorption experiment, the 1876 cm^{-1} species did not show tendency to

form polynitrosyls upon increasing pressure at room temperature. In order to study these apparent contradictions between CO and NO adsorption results we first decided, with the simplest 0.96 wt% Fe-FER sample, to test the hypothesis that the nitrosyl single band at 1876 cm^{-1} may characterize a dinitrosyl species. Indeed, in some specific cases where the angle between the two nitrosyl complexes is 180°, one single active band can be observed by infrared since the coupled symmetric vibration mode becomes IR inactive like in any centro-symmetric system. Note that similar situation is possible with cations exchanged in FER. For instance, there are sites where two NO molecules could approach the cation from different cages [15,16] thus forming linear dinitrosyls. To prove/discard the existence of dinitrosyls we performed isotopically labelled experiments using ^{15}NO–^{14}NO co-adsorption. In the case of dinitrosyl formation each of the expected species $^{14}NO^{14}NO$, $^{15}NO^{14}NO$ and $^{15}NO^{15}NO$ should lead to specific bands (in fact we expect two additional NO stretching modes for the $^{15}NO^{14}NO$ species). Note that, due to relatively strong energetic covalent-like adsorption of NO, formation of dinitrosyls should lead to the splitting of the NO modes (contrary to the case of weak electrostatic adsorption of CO).

Fig. 3 shows the spectrum obtained after introduction of pure ^{15}NO (99% rich) to the 0.96 wt% Fe-FER sample with an equilibrium pressure high enough to ensure the probing of any iron site. The sample was heated at 423 K in order to favour diffusion to all sites and then cooled to r.t. The resulting band at 1842 cm^{-1} is highly symmetric suggesting at first sight one single site. The band position is shifted towards lower wavenumbers (1842 cm^{-1}) with the isotopic shift factor of 1018 as expected [17–19]. This observation is consistent with the results on natural ^{14}NO adsorption on the 0.96 wt% Fe-FER sample.

Let us now consider the spectrum obtained when a gas mixture of both ^{14}NO and ^{15}NO is put in equilibrium with the sample. The experiment was made with first introduction of 133 Pa of ^{15}NO as equilibrium pressure inside the cell and then introduction of ^{14}NO by contacting the cell with an identical volume filled with 133 Pa equilibrium pressure. As a result we only distinguish a second component typical of ^{14}NO nitrosyl (1876 cm^{-1}) without any traces of additional components that would characterize the $^{14}NO^{15}NO$ dinitrosyl species. We then conclude that on our 0.96 wt% Fe-FER sample when NO adsorption is performed at 298–423 K the main species formed are mononitrosyls. At a first sight, the observation that the principal type of Fe^{2+} cations is able to form dicarbonyls with CO, but only mononitrosyls with NO, is contradictory. Note that, due to the strong Fe^{2+}–NO bond, we have performed NO adsorption experiment at room temperature. Usually, at low temperature NO always forms dimers.

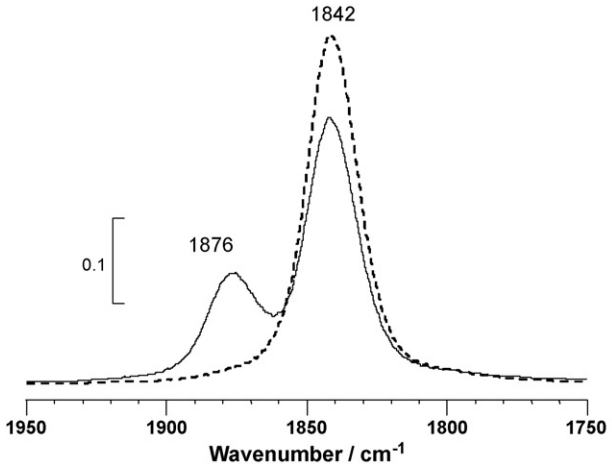

Fig. 3. IR spectra of NO at 298 K on a 0.96 wt% Fe-FER activated under vacuum at 673 K. (- - - -) ^{15}NO equilibrium pressure (133 Pa) and (—) with an equimolar mixture of ^{15}NO and ^{14}NO (partial pressure of each being 67 Pa) after heating at 423 K for 1 h in order to favour the isotopic exchange.

Let us now analyze the intensities of the mono-^{14}NO nitrosyl (1876 cm^{-1}) and mono-^{15}NO nitrosyl bands (1842 cm^{-1}). Although the extinction coefficient of the ^{15}NO nitrosyls is expected to be a little lower [17], the bands should be roughly of the same intensities. Indeed, the spectra show that a band at 1876 cm^{-1} develops after introduction of ^{14}NO to the sample with preadsorbed ^{15}NO and the intensity of the new band roughly corresponds to the diminution of the intensity of the band at 1842 cm^{-1}. The feature is observed after 5 min heating at 423 K but no changes occurred when heating for 1 h at the same temperature.

The unexpected low intensity of the mono-^{14}NO nitrosyl band indicates that the highly symmetric ^{15}NO mononitrosyl envelope is in fact made of at least two components with related species having distinct interaction strengths, one being highly stable and thus hardly isotopically exchanged even at 423 K. This last point is quite important since it indicates that two iron sites produce one single rather symmetric mononitrosyl band, i.e. NO is less directly efficient than CO to evidence different iron sites. Nevertheless a careful analysis of the data permits to have consistent results when comparing the two probe molecules and we can summarize our results for the low loaded 0.96 wt% Fe-FER sample as follows: (i) CO clearly distinguishes two different Fe^{2+} sites directly from distinct carbonyl wavenumbers: the band at 2196 cm^{-1} is typical of monocarbonyl species formed with the most abundant iron sites, which are able to convert to dicarbonyl species at low temperature upon increasing CO pressure; the second band at 2187 cm^{-1} whose intensity is much lower and which is more stable than the previous one (in spite of its lower wavenumber) is assigned to monocarbonyl species formed upon interaction with less abundant iron sites located on more confined sites. (ii) NO hardly differentiates the two distinct iron sites from the nitrosyl wavenumber point of view, however the evolution of the band upon isotopic experiment clearly indicates that at least two iron species leading to two different interaction strengths exist. The fact that these two distinct mononitrosyl species possess almost the same wavenumber but different stabilities is another proof that, as for the case of CO adsorption, some confinement effects occur.

When NO was adsorbed on the 3.7 wt% Fe-FER sample, in addition to the main band at 1876 cm^{-1}, a second ν(NO) component at 1893 cm^{-1} characterizing a third Fe^{2+} site was clearly distinguished. Comparing this observation with the CO adsorption results reported in the previous part, we conclude that the 1876 cm^{-1} main nitrosyl species are formed with the sites that produce the main 2196 cm^{-1} carbonyl band upon CO adsorption. Upon increasing iron loading, two other more confined sites are progressively populated.

These in situ experiments aimed at characterizing the samples and we have provided the results with the two "border" samples having the lowest (characterized by two kinds of Fe^{2+} sites) and highest iron concentration (three types of Fe^{2+}). We have found that Fe gradually occupied different positions in the zeolite with the increasing of the iron loading by consecutive ion exchange. However, it is now established that when the iron loading increases, the formation of iron oxide clusters is favoured and thus it was decided to focus the reactivity study on the 2.5% Fe sample, whose Fe^{2+} distribution is intermediate between these two "border" samples [7].

This characterization part of our work was the first step necessary to probe the iron cations in optimum 'in situ' conditions, i.e. after a vacuum thermal activation enabling the removal of any remaining adsorbed impurities such as water, atmospheric pollutants (VOC...). Indeed without this first knowledge of the

system, it would be almost impossible to extract relevant data from much more complicated (but also realistic) *operando* experiments [1]. The following part of this work thus intend to study the NOx SCR with ammonia using the *operando* methodology, in order to identify the role of the iron sites and their sensitivity to ammonia or SO_2. For sure the characterization of ammonia adsorbed on the acidic sites of the FER structure is also a prerequisite before starting *operando* experiments, however a very elegant and detailed spectroscopic analysis of NH_3 interaction in zeolites was already published [4] and we will rely on.

To start with the ammonia assisted NOx SCR reaction:

$$2NH_3 + 2NO + 1/2O_2 = 2N_2 + 3H_2O \quad (1)$$

we have to remind that in many applications (both stationary and automotive) the NOx species are formed at high temperature upon radical reactions leading to a majority of NO (around 80% of the total NOx). However, it has been widely described that a higher proportion of NO_2 is required for efficient SCR [20–22] according to the reaction:

$$2NH_3 + NO + NO_2 = 2N_2 + 3H_2O \quad (2)$$

and moreover it appears that the NO-to-NO_2 oxidation step would be the SCR rate determining step [23]. That is the reason why we will mainly focus our attention on the evolution of the active red–ox iron sites upon SCR reaction.

3.3. Operando SCR study

With the aim to characterize a potential adsorption competition between the SCR reactants namely NO and NH_3 on the iron sites, we decided to study the reaction in two different ways: (i) first the NO + O_2 flow was sent on the 'as synthesized' FER sample containing both NH_4^+ and Fe^{2+} introduced via ionic exchange; (ii) secondly the NO + O_2 flow was sent on the 'NH_3 reloaded' FER sample on which ammonia flow was previously introduced in order to regenerate the NH_4^+ cations, but eventually producing also NH_3 adsorbed species onto Fe^{2+}.

3.4. SCR reaction with the 'as synthesized' 2.5 wt% Fe-FER

By 'as-synthesized', we mean that the sample was not previously calcined, but according to the preparation procedure, no remaining iron precursor salts are to be expected. In order to remove adsorbed water, the 'as-synthesized' catalyst was simply treated under Argon at the reaction temperature (433 K) for 6 h before the NO + O_2 mixture was sent to the catalyst. Meanwhile the by-passed reactant flow was analyzed in order to check that stable levels are reached before the mixture is sent to the catalyst. Fig. 4 is given in order to illustrate the typical IR spectra we obtained for the gas phase analysis (the bands which are not assigned around 2340 cm^{-1} are typical for gaseous CO_2 that is present in the atmosphere and not as a reaction product). It is thus evident that as soon as the reaction starts (see the arrow) NO is completely removed from the stream whereas the water that is formed upon the SCR reaction (see Eqs. (1) and (2)) appears with a delay. NO_2 formation can also be detected in the exhaust gases after around 60 min. Naturally, some complementary results for a reliable quantitative analysis are obtained from mass spectrometry (such as the m/e = 28 signal which stands in our conditions for N_2 only) and our *operando* system also allows to follow the evolution of typical surface species during reaction. Fig. 5 thus intends to summarize the evolution with time on stream of the main entities (both gaseous and adsorbed) involved during the SCR process. As the m/e = 30 MS signal contains both contributions from NO and NO_2, we decided to follow the NO amount in the gas phase from the

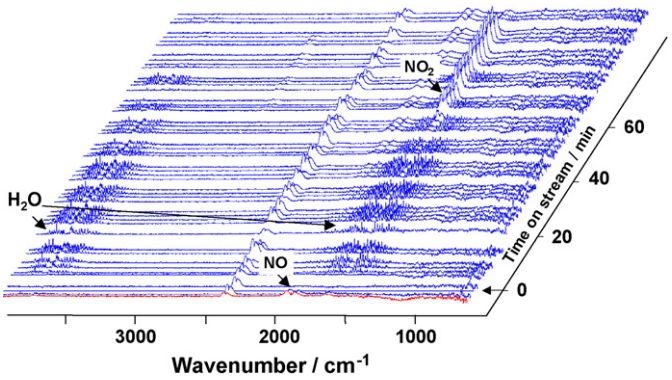

Fig. 4. Gas phase IR spectra acquired during the NO SCR at 433 K (WHSV = 144 h^{-1}) over the 'as synthesized NH_4^+ form' of the 2.5 wt% Fe-FER sample that was previously activated under Ar at 433 K. The arrow indicates the switch from the by-pass to the beginning of the reaction.

IR analysis. We can estimate the instantaneous NO conversion (defined, at any t time on stream, as $\frac{1-[NO_{out}(t)]}{[NO_{in}]}$ to be almost complete (around 95 ± 5%) during the first 30 min on stream, followed by a progressive decrease with stabilization around 35% (pseudo-plateau) after 60 min. As observed from Fig. 4, these 60 min required for NO conversion stabilization correspond to the appearance of NO_2 in the exhaust gas. Regarding the NO_2 quantity, it was decided for sensitivity reason to use the m/e = 46 signal in order to follow its evolution. As indicated in Fig. 5, traces of NO_2 are already present in the reactant flow (around 60 ppm impurities in the lines) but the whole traces disappear as long as the SCR reaction proceeds (as expected from the high reactivity of a NO/NO_2 mixture) and obviously NO_2 starts to be produced when the SCR reaction stops. This last information is extracted from Fig. 5 when considering the evolution of the N_2 amount (m/e = 28 signal): N_2 production from SCR stops after around 60 min. The evolution of the m/e = 18 signal

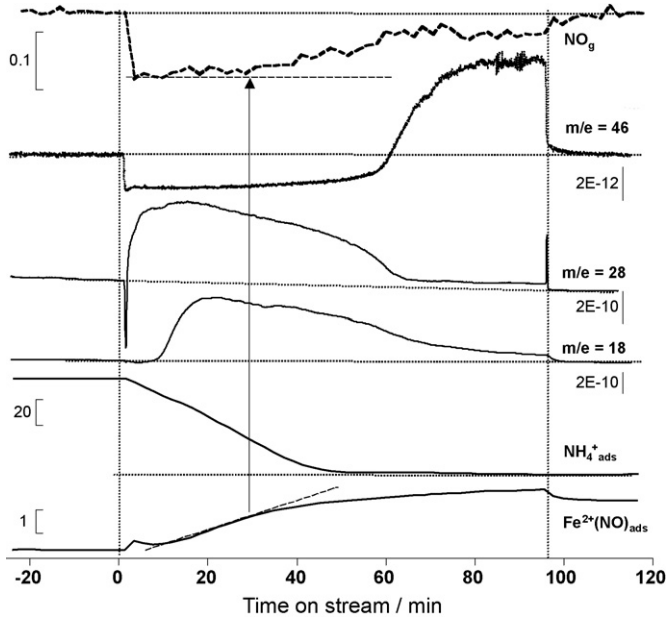

Fig. 5. Chemigrams of typical species involved during the NO SCR at 433 K (WHSV = 144 h^{-1}) over the 'as synthesized NH_4^+ form' of the 2.5 wt% Fe-FER sample previously activated under Ar at 433 K. The data may come from mass spectrometry (as indicated by the m/e signal and its corresponding scale expressed as ion current in A on the right part of the figure) or IR spectroscopy (as indicated by the scale expressed as integrated absorbance in cm^{-1} on the left part of the figure). Reaction starts at t = 0 min and flow is by-passed at t = 95 min.

relative to the water that is co-produced during the SCR confirms this conclusion. Indeed, water detection in the gas phase is delayed when compared to N_2, but this can be easily explained by water adsorption until a surface equilibrium is reached. Summarizing all these gas data, one can conclude that, in water free conditions, this catalyst is highly efficient for NOx removal showing an initial maximum NOx elimination around 95% with a very high selectivity to N_2 and a SCR global efficiency of 75% during 60 min. The SCR global efficiency was calculated as follows:

$$\int_{t_0}^{t_{\text{end of SCR}}} \frac{[NO_{\text{in}}] - [NO_{\text{out}}(t)]}{[NO_{\text{in}}]}\, dt,$$

but it may be more useful to determine the total amount of eliminated NO until NH_4^+ species is fully consumed. Considering that in our experimental conditions, we have a NO flow $F_{NO} = 1.8 \times 10^{-3}$ mol g^{-1} h^{-1}, we find a value of eliminated NO equal to 1.35×10^{-3} mol g^{-1}. This value is fully consistent with the theoretical one, which is expected to be slightly lower than the total ionic exchange capacity of 1.7×10^{-3} mol taking into account that iron cations are present together with ammonium species. A precise value of the initial NH_4^+ amount is hard to obtain from our actual data since both Fe^{2+} and Fe^{3+} are present in the sample and only the global Fe/Al ratio is available. As soon as the SCR reaction stops, the NO-to-NO_2 oxidation reaction is observed with a 35% yield.

Considering now the catalyst study under duty, we decided to focus on the two main surface species, i.e. ammonium ions (NH_4^+) and iron nitrosyls [Fe^{2+}(NO)]. Dealing with the methodology, the complex ammonium δ(NH) massif area was integrated in the 'wide' range [1550–1304 cm^{-1}] in order to follow the global evolution of this species and the same choice was made for the nitrosyl band, whose integration was achieved in the 'wide' [1946–1816 cm^{-1}] range. It is clear from Fig. 5 that as soon as N_2 is produced, NH_4^+ species disappear. This is consistent with the fact that the SCR mechanism proceeds via chemisorbed ammonia species and that in one produced N_2 molecule one nitrogen atom comes from NO and the second one from NH_3 as it was elegantly reported using isotopic exchange reaction [24]. Moreover, considering the monotonous decrease of the NH_4^+ species amount with time on stream, it appears that the ammonium disappearance rate ($-$d[NH_4^+]/dt) is constant. Since the NO conversion varies especially after 30 min on stream (and thus the SCR reaction rate), we can conclude that the surface reaction between adsorbed ammonia species and NOx is not the rate determining step. On another hand, focusing on the evolution of the iron nitrosyl species, we can clearly observe a decrease of the slope (d[$Fe^{2+}(NO)_{ads}$]/dt) after around 30 min, time from which both the NO conversion, the N_2 and the water production decrease (so the SCR rate decreases). This clearly indicates a key role of the iron nitrosyls for the SCR reaction. In this frame, we can notice that when the NO_2 yield has stabilized to around 35% (after 80 min) the $Fe^{2+}(NO)_{ads}$ amount has reached a plateau.

3.5. SCR reaction with the 'NH$_3$ reloaded' 2.5 wt% Fe-FER

The SCR reaction is classically operated when sending both NH_3 and NO to the catalyst, but in this case the study of the system is complicated since both reactants may compete for the same iron adsorption site. In the previous part, we were able to get rid of NH_3 adsorption onto iron by using the 'as-synthesized' NH_4^+ form of the 2.5 wt% Fe-FER sample. Now, we will consider the differences we may obtain when studying the SCR reaction after the same sample has been reloaded under a NH_3 flow at 433 K and further maintained under a pure argon flow at the same temperature until no more ammonia desorption was detected. This point is quite important to only keep as adsorbed species the stable ones

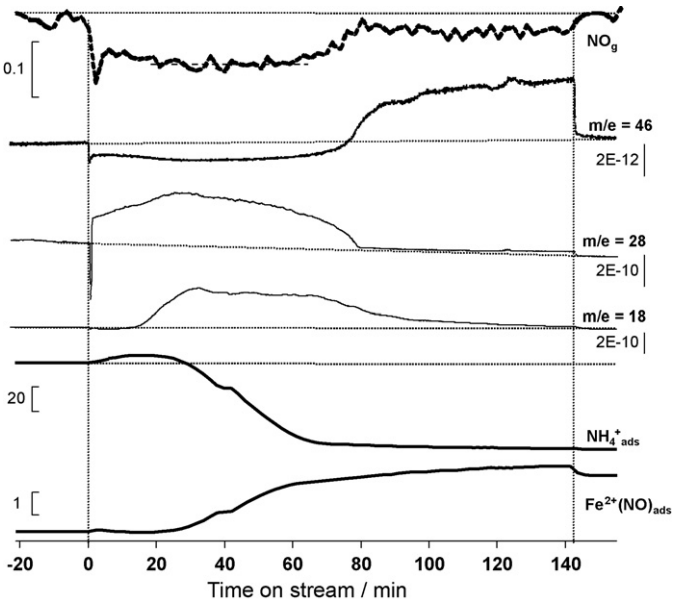

Fig. 6. Chemigrams of typical species involved during the NO SCR at 433 K (WHSV = 144 h^{-1}) over the 'NH$_3$ reloaded' 2.5 wt% Fe-FER sample previously maintained under Ar at 433 K for 220 min. The data may come from mass spectrometry (as indicated by the m/e signal and its corresponding scale expressed as ion current in A on the right part of the figure) or IR spectroscopy (as indicated by the scale expressed as integrated absorbance in cm^{-1} on the left part of the figure). Reaction starts at t = 0 min and flow is by-passed at t = 145 min.

for a given temperature and then establish whether or not there is NH_3 slip when switching to SCR reaction flow. As for the previous experiment, Fig. 6 compiles the data obtained from the different techniques. The gas phase analysis indicates similar behaviors but with rather distinct shapes for the various signals. Indeed, NO is never completely consumed and its maximum conversion ($80 \pm 5\%$) is not reached from the first instance of reaction but between 20 and 50 min on stream. More precisely it appears that there is an induction period for both NO and NO_2 (impurities in the lines) since their respective conversion increases with time during the first 20 min on stream. The increase of the SCR reaction rate during the first instant of reaction is confirmed by the N_2 (m/e = 28) evolution shape which also indicates that the duration for which the SCR reaction proceeds increased from 60 to 80 min. We shall also note here that the global SCR efficiency slightly decreased ($65 \pm 5\%$) but that the total amount of eliminated NO increased (when compared with the as synthesized sample) to 1.56×10^{-3} mol g^{-1}. This quantitative result is consistent with a higher amount of stored NH_3, which adsorbed both onto Brønsted acidic sites (forming ammonium ions) and iron cations upon reloading. When the SCR was finished, we also measured a lower NO-to-NO_2 oxidation capacity of 25%. Since it was reported in the literature that the presence of NO_2 in the NOx flow was detrimental to the NO-to-NO_2 reaction rate on Fe-MFI zeolites [25], we compared the amount of NO_2 impurities in the lines for this experiment (30 ppm) with the one measured for the as-synthesized sample experiment (60 ppm). The conversion lost after NH_3 reloading can thus not be associated to an NO_2 inhibiting effect. Finally, as for the previous case, no ammonia slip was detected in the exhaust gas (data not shown).

For a given stable catalyst, it makes no sense to observe an increasing reaction rate with time on stream, our result would thus indicate that the amount of active catalytic centres increases with time on stream. In order to check this hypothesis, we considered again the evolution of the main surface species when the catalyst is under duty. In contrast to the reaction made with the 'as-synthesized' sample, we surprisingly observed here an increase of the NH_4^+ amount for the first instants of reaction. This

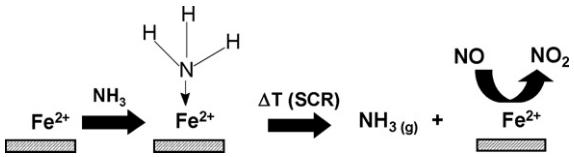

Scheme 1. A model for the NH_3 effect on iron sites.

phenomenon is to be correlated with the absence of $Fe^{2+}(NO)_{ads}$ during the same period. Indeed, as there is no NH_3 in our reaction flow, we propose according to Scheme 1 that after ammonia reloading the iron sites are 'poisoned' by coordinated NH_3, then when the NO + O_2 mixture is sent to the catalyst the 'slow' SCR reaction described by Eq. (1) starts and the associated exothermicity provokes the decomposition of the $Fe(NH_3)_{ads}$ species, thus releasing gaseous ammonia which is trapped by both free acidic sites and non-coordinatively saturated ammonium species (mono-to-tridentate species according to Ref. [4]). We made an attempt to directly confirm this proposal by focusing on the $Fe(NH_3)_{ads}$ signal, however we do not report any evolution of this region (1600–1640 cm^{-1}) with time on stream since the overall band intensity increases with the only formation of water upon SCR reaction and thus no conclusion can be drawn regarding the reactivity of Lewis bonded NH_3 species.

However, Scheme 1 is consistent with an increase of the amount of active catalytic centres during the first instants, since as soon as iron sites are free from adsorbed NH_3 they become available for NO adsorption to yield NO_2 and thus the 'fast' SCR reaction (described by Eq. (2)) starts. The nice time coincidence between the appearance of $Fe^{2+}(NO)_{ads}$ and the appearance of the maximum SCR rate (after around 20 min on stream) confirms this hypothesis. Finally, we must also notice that when the NO-to-NO_2 reaction reaches a pseudo-stable value (after that the SCR reaction has consumed the totality of the $NH_4^+{}_{ads}$ species), the final integrated area corresponding to the $Fe^{2+}(NO)_{ads}$ species also reaches a plateau level, whose value is very similar (even a little bit higher) to the one obtained in the previous study (see Fig. 5 for comparison). In the case the rate determining step for the SCR reaction was the catalytic NO-to-NO_2 reaction, one should expect this NO-to-NO_2 reaction rate to be the same when the SCR is finished, at least as far as the catalytic centres are identical. Indeed, we should expect to obtain the following law: $dNO_2/dt = k[Fe^{2+}(NO)_{ads}]$ when the NO oxidation alone takes place. At a first sight, this is not what we actually observe, since when decreasing from 35% NO_2 yield (Fig. 5) to 25% (Fig. 6), the total integrated area for the global $Fe^{2+}(NO)_{ads}$ species slightly increased. However, a great care should be taken when concluding from the previous results since they are not intrinsically sufficient to reject the hypothesis of NO to NO_2 being the rate determining step. Effectively for data processing facilities reasons, the massif corresponding to the ν(NO) vibration of $Fe^{2+}(NO)_{ads}$ species was globally integrated, whereas we demonstrated in the previous part of this study that at least three distinct iron sites are present. Indeed, these distinct iron sites lead to distinct nitrosyl species with very 'close' wavenumber and for which the less intense would characterize the iron red–ox most active site [7]. It is thus possible that in the case of the 'NH_3 reloaded' experiment, part of the iron active site has been poisoned leading to lower NO-to-NO_2 conversion, which has to be associated to a lower amount of 'active $Fe^{2+}(NO)_{ads}$'. This lower amount of 'active $Fe^{2+}(NO)_{ads}$' would not be detected since the signal corresponding to 'spectator $Fe^{2+}(NO)_{ads}$' is much more intense. Moreover, the presence of adsorbed water may lead to partially poisoned iron sites, which would still be able to co-adsorb NO but with different corresponding wavenumber and molar extinction coefficient [7,26]. Thus different amounts of adsorbed water may also explain different global integrated intensities for the $Fe^{2+}(NO)_{ads}$ massif when the NO-to-NO_2 reaction reached a steady state. In order to obtain more details concerning the so-called 'rate determining step' NO-to-NO_2 reaction, we decided to study this reaction in optimized conditions.

3.5.1. Operando NO-to-NO_2 study in steady state conditions

For this purpose, a new Fe-FER sample was thermally activated at 673 K under pure argon in order to convert it from the NH_4^+ as-synthesized form to the H^+ (non-SCR active) form and to remove any adsorbed water. The sample was further cooled down to the reaction temperature (433 K) under the same dry argon flow and the NO + O_2 flow was sent to the catalyst. The online analysis of the gas phase indicated a rather good NO oxidation efficiency at steady state for this new Fe-FER sample (around 50% NO conversion at 433 K). Focusing on the surface analysis during the NO oxidation reaction, Fig. 7 shows the spectra obtained for different flow conditions. Both temperature and flow composition were kept constant but the contact time was doubled by changing the weight hourly space velocity (350 $h^{-1} \rightarrow 175\ h^{-1}$). At constant NO partial pressure, the conversion increased from 43% to 50%. Since these conversion levels are too high to consider the reactor working as a differential one, we will not attempt to determine the reaction rates but will consider the catalyst activity (NO_{in} flow/catalyst weight × conversion): $A_a = 500 \times 10^{-6} \times 350/40 \times 0.43 = 1.88 \times 10^{-3}$ mol of transformed NO into NO_2 per gram of catalyst and per hour and $A_b = 500 \times 10^{-6} \times 175/40 \times 0.5 = 1.09 \times 10^{-3}$ mol $g^{-1}\ h^{-1}$. We then observe for the **b** experiment (with the lowest activity), a decrease of the intensity of the nitrosyl massif (band centred around 1875 cm^{-1}). Indeed, the steady state being reached and considering an elemental slice of catalyst volume dV in which the NO_2 is produced according to: $d(NO_2) = k_r(NO)_{ads}dV$ [thus considering $(NO)_{ads}$ as intermediate species], the integration on the whole catalyst volume leads to: $NO_{2out} - NO_{2in} = k_r(NO)_{ads.tot}$, which is completely equivalent to NO_{in} × conversion = $k_r(NO)_{ads.tot}$ [where k_r stands for the pseudo-rate constant including the O_2 concentration in high excess, $(NO)_{ads}$ stands for the amount of adsorbed mononitrosyl in the dV slice and $(NO)_{ads.tot}$ for the total amount of adsorbed mononitrosyls in the whole catalyst volume which is crossed by the infrared beam]. In these optimized conditions for which no NH_3 poisoning or adsorbed water effect could be evocated, our data thus allow us to conclude that the 'whole $Fe^{2+}(NO)_{ads}$ species' follow the same evolution than reaction intermediates: the catalyst activity decreases when the amount of mononitrosyls decreases. Moreover, without any kinetic considerations, we must emphasise that working at constant NO partial pressure and

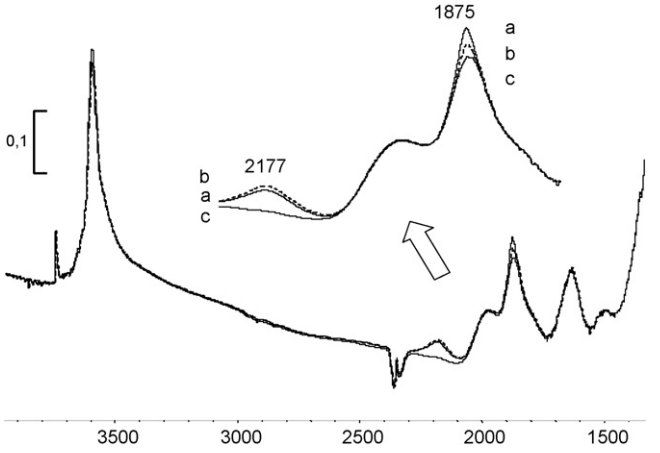

Fig. 7. Surface IR spectra for the best Fe-FER sample in NO-to-NO_2 reaction at 433 K, flow: (a) 500 ppm NO, 6% O_2 in Ar, WHSV = 350 h^{-1}, (b) identical except WHSV = 175 h^{-1}, and (c) pure Ar.

temperature, the amount of purely spectator adsorbed species should reach the same level at steady state, which was obviously not the case for our $Fe^{2+}(NO)_{ads}$ species. Our previous in situ NO adsorption experiments indicated that for all Fe-FER samples (whatever the iron loading) the main nitrosyl band is located at 1876 cm^{-1} at room temperature. However, it is known that for one given species, the corresponding infrared bands wavenumbers are temperature dependent: the highest the temperature, the lowest the wavenumber. Moreover, we also evidenced in the previous NO adsorption study that the main nitrosyl band at 1876 cm^{-1} is in fact typical of two distinct iron sites! In these conditions, it is thus very difficult to establish whether or not one specific iron site is involved in the NO oxidation and for sure even more delicate to conclude which one. Some investigations are under current study in order to try to poison selectively one type of Fe^{2+} and to conclude using the so-obtained *operando* results. However, one can actually propose, according to these first results, that when in optimized conditions the whole Fe^{2+} sites may be active centres for NO-to-NO_2 oxidation, whereas when going to realistic conditions (the catalyst being in contact with NH_3 and water) some partial poisoning phenomena may exist leading to both 'active $Fe^{2+}(NO)_{ads}$' and 'spectator $Fe^{2+}(NO)_{ads}$' species.

At this step of the study, it is necessary to discuss the nature of the iron active sites. Indeed, as far as the NO-to-NO_2 reaction is concerned, we are dealing with a red–ox catalytic cycle in which the transition metal oxidation number varies. Depending on the technique that is used, some scientists will conclude that the presence of Fe^{3+} in cationic sites (as detected by UV–vis or EPR for instance) is essential for the oxidation of NO into NO_2 [25], while others will consider Fe^{2+} as the active species (as concluded in this work). We do believe that none of the previous conclusions is wrong and we must indeed remind that among the Fe^{2+} and Fe^{3+} species only those whose both the oxidation and the coordination states may change easily are excellent candidates for active redox sites. In our case, using IR spectroscopy, we only detect the $Fe^{2+}(NO)_{ads}$ active species before Fe^{2+} are oxidized to Fe^{3+} which do not interact anymore with NO [7].

Going on with the description of Fig. 7, we observe the simultaneous appearance of another band centred at 2177 cm^{-1} which can be assigned to the NO^+ molecular cations [18,27]. This NO^+ species is formed from NO_2 [9,10] and it is thus logical to observe an increased amount of adsorbed species when the conversion increases and thus when the local NO_2 partial pressure increases. Spectrum c characterizes the surface after 4 min under pure Ar at 433 K (after reaction): both components at 2177 and 1875 cm^{-1} quickly decrease (there is a structural combination band beneath the 1875 cm^{-1} mononitrosyl one), which indicates that the corresponding species are little stable. We do conclude from all these results that iron mononitrosyl species (at least one in realistic conditions) are active species for NO oxidation into NO_2.

3.5.2. *Operando study of the SO_2 effect on NO oxidation to NO_2*

Finally, we must remind that the actual trend to develop SCR process for automotive exhaust gases treatment is both justified by the need to operate at lower and lower temperature (around 523 K) at which the actual NOx trap catalysts are not efficient enough and by the fact that these NOx trap catalyst are highly sensitive to the presence of sulphur. We thus decided to test the potential poisoning effect of SO_2 on our Fe-FER catalyst during the NO-to-NO_2 reaction. We focused on this reaction because our results are consistent with literature data indicating that it is the rate determining step during the SCR reaction. Indeed, we were not able to really identify which of the various Fe^{2+} sites is/are active during the SCR reaction but: (i) a constant ammonium disappearance rate ($-d[NH_4^+]/dt$) while the NO_g disappearance rate ($-d[NO_g]/dt$) varies (see Fig. 5) indicates that surface reaction between NO and NH_4^+ is not the rate determining step and (ii) the fact that the maximum SCR efficiency decreases when the NO-to-NO_2 efficiency decreases (compare Figs. 5 and 6) is consistent with the NO oxidation being considered as the rate determining step.

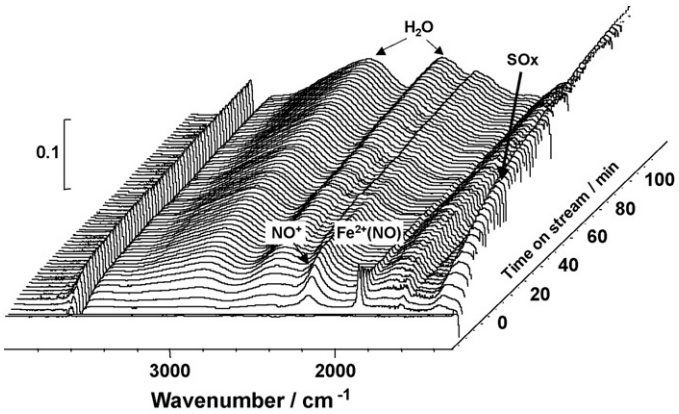

Fig. 8. Evolution of the catalyst IR surface spectra during the NO-to-NO_2 reaction at 433 K (with SO_2) over the 2.5 wt% Fe-FER sample previously activated under Ar at 433 K for one night. The spectrum of the 'by-passed' catalyst surface was subtracted for clarity seek so that positive bands correspond to species formed upon reaction whereas negative bands characterize species disappearing upon reaction.

Fig. 8 reports the surface spectra (the spectrum corresponding to the 2.5 wt% Fe-FER in the H^+ form under pure Ar was subtracted for clarity seek) obtained when 50 ppm of SO_2 was added in the NO + O_2 flow. It is obvious that NO adsorption onto Fe^{2+} initially takes place with further oxidation to NO_2, which is required to form the NO^+ cations that are also initially detected. The NO^+ formation could go through different mechanisms involving NO_2: (i) reaction with acidic OH groups [18] leading to water formation (as detected) and (ii) NO_2 dismutation, which produces nitrates [19] that are also initially detected with a broad band around 1375 cm^{-1}. However, this nitrate band very quickly enlarges towards lower wavenumbers with a new maximum around 1300 cm^{-1} that should be associated to adsorbed SOx species

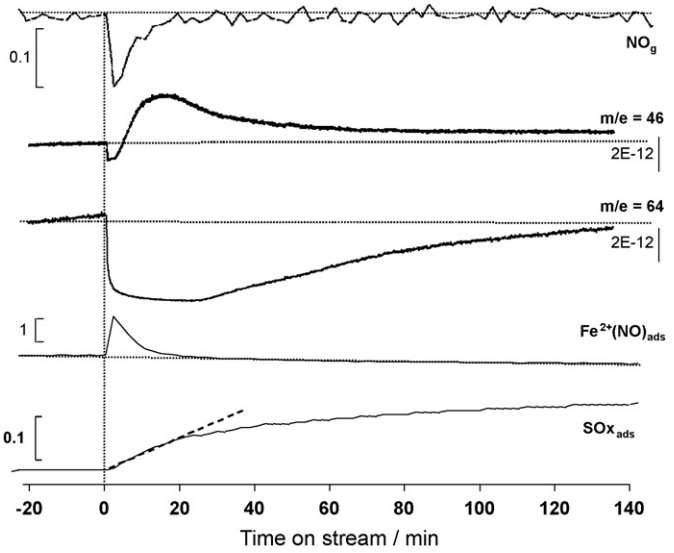

Fig. 9. Chemigrams of typical species involved during the NO-to-NO_2 reaction at 433 K (with SO_2) over the 2.5 wt% Fe-FER sample previously activated under Ar at 433 K for one night. The data may come from mass spectrometry (as indicated by the *m/e* signal and its corresponding scale expressed as ion current in *A* on the right part of the figure) or IR spectroscopy [as indicated by the scale expressed as integrated absorbance in cm^{-1} (except for the SOx_{ads} signal for which height of the peak in a.u. is reported) on the left part of the figure].

most probably in the sulphate form [27]. Fig. 9 compiles again the results from both the gas phase and the surface analysis. The m/e = 64 signal's evolution confirms that SO_2 disappears from the gas phase to be kept on the surface as adsorbed species. Moreover, considering the initial slope of the SOx_{ads} signal, we can conclude that the higher SOx adsorption rate corresponds to the total SO_2 removal from the gas phase (during around the first 25 min on stream). Moreover, when the SO_2 level at the exit of the reactor cell reaches the same value that the one at the inlet, the SOx_{ads} signal tends to a plateau. This further confirms our assignment of the 1300 cm^{-1} component to SOx containing species (most probably sulphate) which accumulate on the surface. Dealing now with the evolution of the NO_g signal, we observe a very fast initial decrease, but after around 15 min the NO amount reaches almost the same level (according to the IR noise) as the one detected when the catalyst is by-passed. If we focus on the '$Fe^{2+}(NO)_{ads}$' signal we realize that its intensity is going though a maximum to quickly tends to 0. The time corresponding to this maximum perfectly matches with the minimum of the NO_g signal and the beginning of NO_2 detection. It thus appears that we first only observe pure adsorption of NO from the gas phase to form '$Fe^{2+}(NO)_{ads}$', which are further oxidized into NO_2 (which appears with a delay in the gas phase because it is initially involved in the formation of the NO^+ species detected on the surface). This is also an indirect confirmation of the role of Fe^{2+} cations as active sites for the NO-to-NO_2 oxidation. However, most of the Fe^{2+} sites are not regenerated to become available for new adsorption of NO and maintain the reaction since they are poisoned by sulphates species formation. Indeed, the appearance of SOx_{ads} species corresponds to the decrease of the '$Fe^{2+}(NO)_{ads}$' signal. Nevertheless, it appears to us that a minor part of Fe^{2+} in the FER structure is thioresistant since the highly sensitive mass spectrometry indicates that under steady state (after the poisoning has stabilized) the NO conversion to NO_2 still goes on (even with a low value of 4%).

4. Conclusions

As indicated by the necessary preliminary characterization studies, the main fraction of Fe^{2+} cations exchanged in Fe-FER is located in non-confined sites. These Fe^{2+} cations are coordinatively unsaturated, i.e. they can easily form dicarbonyls. Small fraction of two distinct more acidic Fe^{2+} cations, located in more confined/smaller cavities, are also present and their relative concentration increases with the number of successive exchange procedures.

Operando studies indicate that our samples present interesting NOx SCR efficiency for temperature as low as 433 K. Our results also indicate that for such low reaction temperature ammonia and nitrogen monoxide compete for adsorption onto Fe^{2+} species, which are active for the NO-to-NO_2 oxidation. Our results are also consistent with this last reaction being the rate determining step of the global SCR process and we finally concentrated our study on the effect of SO_2 on this NO-to-NO_2 reaction. We must conclude that for the 2.5 wt% Fe-FER sample, the majority of iron sites are poisoned by sulphates formation, however and to finish with an optimistic point of view, some Fe^{2+} sites are thioresistant. Our aim is now to identify them and to find a way to increase their proportion in the FER structure.

Acknowledgments

The in situ part of this work was performed in the framework of the RILA French–Bulgarian cooperation. E.I. is grateful to the French Ministry of Higher Education and Research for a 1-year postdoctoral fellowship. K.H., E.I. and M.M also acknowledge support from the Bulgarian Scientific Fund (grant DO 02-184). The *operando* part of this study was partially supported by the French Agency for Energy and Environment (ADEME) and by the French Department for Industry.

References

[1] P. Bazin, O. Marie, M. Daturi, Stud. Surf. Sci. Catal. 171 (2007) 97.
[2] Y. Li, J.N. Armor, Appl. Catal. B: Environ. 1 (1992) 31.
[3] K. Hadjiivanov, G. Vayssilov, Adv. Catal. 47 (2002) 307.
[4] A. Zecchina, L. Marchese, S. Bordiga, C. Pazè, E. Gianotti, J. Phys. Chem. B 101 (1997) 10128.
[5] T. Lesage, C. Verrier, P. Bazin, J. Saussey, M. Daturi, Phys. Chem. Chem. Phys. 5 (2003) 4435.
[6] T. Lesage, C. Verrier, P. Bazin, J. Saussey, S. Malo, C. Hedouin, G. Blanchard, M. Daturi, Topics Catal. 30/31 (2004) 31.
[7] V. Blasin-Aube, O. Marie, J. Saussey, A. Plesniar, M. Daturi, N. Nguyen, C. Hamon, M. Mihaylov, E. Ivanova, K. Hadjiivanov, J. Phys. Chem. C 113 (2009) 8387.
[8] E. Paukshtis, R. Soltanov, E. Yurchenko, React. Kinet. Catal. Lett. 22 (1983) 147.
[9] S. Bordiga, E.E. Platero, C.O. Arean, C. Lamberti, A. Zecchina, J. Catal. 137 (1992) 179.
[10] C.O. Arean, O.V. Manoilova, M.R. Delgado, A.A. Tsyganenko, E. Garrone, Phys. Chem. Chem. Phys. 3 (2001) 4187.
[11] K. Hadjiivanov, E. Ivanova, M. Kantcheva, E. Cifitikli, D. Klissurski, L. Dimitrov, H. Knözinger, Catal. Commun. 3 (2002) 313.
[12] M.N. Bae, M.K. Song, Y. Kim, K. Seff, Micropor. Mesopor. Mater. 63 (2003) 21.
[13] K. Hadjiivanov, E. Ivanova, H. Knözinger, Micropor. Mesopor. Mater. 58 (2003) 225.
[14] P. Nachtigall, R. Bulánek, Appl. Catal. A 307 (2006) 118.
[15] R. Bulanek, I. Voleska, E. Ivanova, K. Hadjiivanov, P. Nachtigall, J. Phys. Chem. C 113 (2009) 11066.
[16] K. Chakarova, K. Hadjiivanov, Micropor. Mesopor. Mater. 123 (2009) 123.
[17] S. Pinchas, L. Laulicht, Infrared Spectra of Labelled Compounds, Academic Press, London/New York, 1971.
[18] K. Hadjiivanov, J. Saussey, J.L. Freysz, J.C. Lavalley, Catal. Lett. 52 (1998) 103.
[19] C. Henriques, O. Marie, F. Thibault-Starzyk, J.C. Lavalley, Micropor. Mesopor. Mater. 50 (2001) 167.
[20] A. Kato, S. Matsuda, T. Kamo, J. Phys. Chem. 85 (1981) 4099.
[21] G. Madia, M. Koebel, M. Elsener, Ind. Eng. Chem. Res. 41 (2002) 3512.
[22] O. Kröcher, Stud. Surf. Sci. Catal. 171 (2007) 261.
[23] R.Q. Long, R.T. Yang, J. Catal. 207 (2002) 274.
[24] G. Li, C.A. Jones, V.H. Grassian, S.C. Larsen, J. Catal. 234 (2005) 401.
[25] R. Brosius, D. Habermacher, J.A. Martens, L. Vradman, M. Herskowitz, L. Capek, Z. Sobalik, J. Dedecek, B. Wichterlova, V. Tokarova, O. Gonsiorova, 6th International Congress on Catalysis and Automotive Pollution Control (CAPoC6), Springer, Brussels, Belgium, October 22–24, 2003.
[26] K. Hadjiivanov, D. Klissurski, G. Ramis, G. Busca, Appl. Catal. B: Environ. 7 (1996) 251.
[27] R.Q. Long, R.T. Yang, J. Catal. 194 (2000) 80.